RESEARCH   **Open Access**

Wear-resistant surface coloring by ultrathin optical coatings

Jiao Geng[1,2], Liping Shi[1,2]* ⓘ, Junhuan Ni[1,2], Qiannan Jia[1,2], Wei Yan[1,2] and Min Qiu[1,2]*

*Correspondence:
shiliping@westlake.edu.cn;
qiumin@westlake.edu.cn
[1]Key Laboratory of 3D Micro/Nano Fabrication and Characterization of Zhejiang Province, School of Engineering, Westlake University, Hangzhou, China
[2]Institute of Advanced Technology, Westlake Institute for Advanced Study, Westlake University, Hangzhou, China

Abstract

We design, fabricate, optically and mechanically characterize wearable ultrathin coatings on various substrates, including sapphire, glass and silicon wafer. Extremely hard ceramic materials titanium nitride (TiN), aluminium nitride (AlN), and titanium aluminium nitride (TiAlN) are employed as reflective, isolated and absorptive coating layer, respectively. Two types of coatings have been demonstrated. First, we deposit TiAlN after TiN on various substrates (TiAlN-TiN, total thicknesses <100 nm), achieving vivid and viewing-angle independent surface colors. The colors can be tuned by varying the thickness of TiAlN layer. The wear resistance of the colorful ultrathin optical coatings is verified by scratch tests. The Mohs hardness of commonly used surface coloring made of Si-/Ge-metals on substrates is <2.5, as soft as fingernail. However, the Mohs hardness of our TiAlN-TiN on substrates is evaulated to be 7-9, harder than quartz. Second, Fano-resonant optical coating (FROC), which can transmit and reflect the same color as a beam split filter is also obtained by successively coating TiAlN-TiN-AlN-TiN (four-layer film with a total thickness of 130 nm) on transparent substrates. The FROC coating is as hard as glass. Such wearable and color-tunable thin-film structural colors and filters may be attractive for many practical applications such as sunglasses.

Keywords: Abrasion-resistance optical films, Structural colors, Fano-resonance, Titanium aluminium nitride (TiAlN)

Introduction

In the colorful world we are living, the vivid colors always bring beauty and pleasure. The colors in nature usually originate from three sources including pigments, bioluminescence, and structural colors [1–6]. The last one, arising from surface structures, have attracted considerable interests in recent years. Their fascination does not only reproduce the brilliant natural examples, but also offer versatile applications in bio-inspired functional photonic materials [7–9]. The structural colors can be produced by various mechanisms, such as surface plasmon resonances [10–18], Mie-type scattering by all-dielectric nanoparticles [19, 19–24], diffractive structures [25–28], or thin-film interference [29–32]. From the standpoint of manufacturability, the thin film-induced structural colors are advantageous for macro-fabrication and integration into devices, as they do not require complex nanofabrication methods such as lithography, etching, milling or femtosecond laser writing [33, 34].

Recently, a type of optical coating called thin-film absorber is of interest for surface coloring [35, 36]. Such coating consists of an ultrathin semiconductor film with strong optical loss deposited on a highly reflective metallic film (semiconductor-metal coating: SM). It should be noted that the colors of SM coatings are independent of viewing angles. Upon the SM coating, Fano-resonant optical coating (FROC) has been demonstrated more recently [37], which relies on Fano resonance that occurs when a narrowband resonance is coupled with a broadband resonance [38]. In FROC, the SM acts as a broadband absorber coupling with a metal-dielectric-metal (MDM) cavity as a narrowband light absorber. The SM and MDM resonators share a same metallic layer. The unique feature of FROC is that it transmits and reflects the same color, which is hard to realize in the conventional optical coatings.
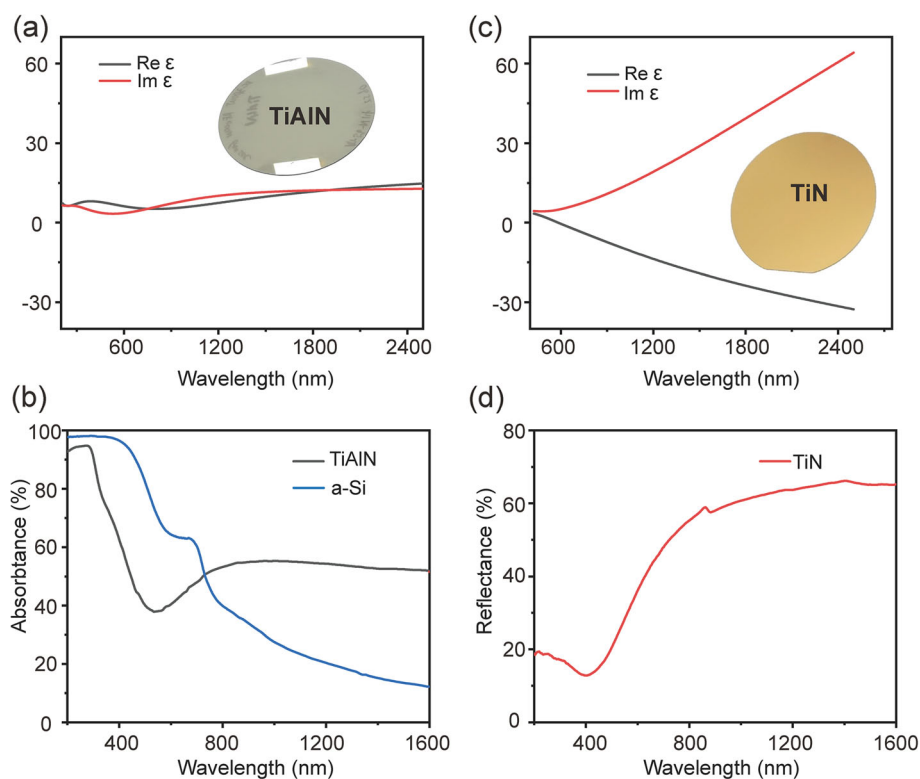
In practical applications, the durability of the structural colors is of concern. For instance, their resistance to mechanical abrasion is vital for decoration technologies. Compared with other micro/nanostructure-based coloring techniques, the thin-film optical coatings are certainly more durable. However, silicon (Si) and Germanium (Ge) are often employed as the absorbing layer; noble metals like gold (Au), silver (Ag), copper (Cu) and aluminium (Al) are usually utilized as the reflective layer [35, 37]. These materials are not robust enough to withstand mechanical abrasion [39, 40].

Here, we demonstrate wearable SM- and FROC-type surface coloring coatings based on extremely hard ceramic materials including TiN, AlN and TiAlN. As an alternative to noble metals, metallic TiN is adopted, functioning as the reflective layer. In addition, TiAlN, instead of Ge or Si is chosen as the absorbing layer. TiN and TiAlN with a thickness of several micrometers are usually utilized as hard coatings for mechanical workpieces, which significantly improve the material performance in cutting, molding and casting manufacture processes and play important roles in automotive and aerospace industries) [41–44]. Nevertheless, application of these hard materials as ultrathin optical coatings for surface coloring is rarely explored [45]. What's more, the wear resistance of these materials with an overall thickness of a few tens of nanometers remains unclear.

Results and discussion

TiAlN and TiN thin films can be deposited on various substrates using magnetron reactive sputter. Figure 1a and c plot their real (Re ϵ) and imaginary (Im ϵ) parts of the extracted dielectric functions, respectively. TiAlN manifests as a highly lossy dielectric (Fig. 1b). Its Re ϵ is positive, and Im ϵ is large in the visible and near-infrared spectral ranges (Fig. 1a). Therefore, as shown in the inset of Fig. 1a, a 50-nm-thick TiAlN film on glass substrate presents a gray color. The absorbance of TiAlN in the visible spectral range is comparable to that of amorphous silicon (a-Si) with the same thickness (Fig. 1b), rendering it as an excellent alternative for SM-type surface coloring. Unlike TiAlN, TiN film behaves as a metallic material and displays a golden color (inset in Fig. 1c). Its screened plasma wavelength is measured to be at ~600 nm. The large negative values of Re ϵ above 600 nm indicate that it is highly metallic in the near-infrared regime.
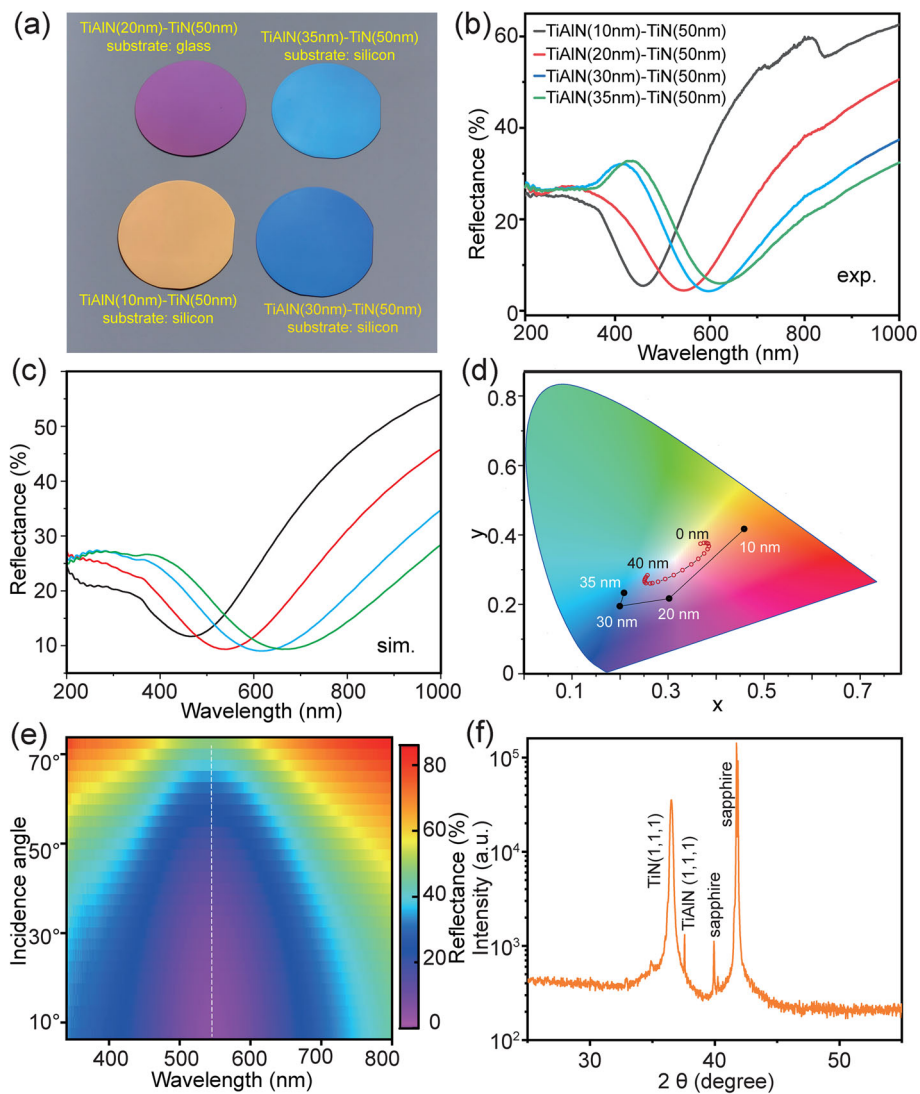
Although the reflectance of TiN in the visible spectral range (Fig. 1d) is much lower than that of Au, Ag, Cu or Al, it can still be used as a reflective layer for SM-type surface coloring. When successively depositing TiAlN and TiN films on substrates, the bilayer TiAlN-TiN displays vivid structural colors (Fig. 2a). Increasing TiAlN thickness from 10 to 35 nm, several colors including yellow, violet, cerulean and light blue are observed.

Fig. 1 Measured dielectric constant of TiAlN film (**a**) on a glass substrate, and TiN (**c**) on a silicon wafer. Re ϵ: real part of permittivity; Im ϵ: imaginary part of permittivity. Insets: photographs of 50-nm-TiAlN and 50-nm-TiN films on a glass and silicon substrate, respectively. **b**, absorption spectra of 50-nm-thick TiAlN (black curve), and 50-nm-thick a-Si (blue curve). **d**, Reflectance spectrum of 50-nm-TiN film sputtered on a silicon wafer at 300 ℃

At normal incidence, the reflectance spectra of the bilayer TiAlN-TiN redshifts with the increased thickness of TiAlN layer (Fig. 2b). This is in agreement with the numerical simulations (Fig. 2c). Plotting the measured spectra (Fig. 2b) on the CIE 1931 color space, the corresponding chromaticities (black dots in Fig. 2d) match well with the observed colors in Fig. 2a. However, the simulated gamut (red dots in Fig. 2d) is narrower than the measured one. This may be attributed to the fact that the permittivity of TiAlN for simulation is retrieved after it is deposited on glass substrates, which differs from that on TiN substrates. As TiAlN coatings are much thinner than the wavelength of light, compared with the case of reflection, there is little phase accumulation due to the propagation through the film. The resonant dips of the reflectance spectra remain unchanged for incidence angles ranging from 6° to 75° (dashed line in Fig. 2e and Supplementary Fig. S1). Therefore, the structural colors originating from the bilayer SM-films are independent of the viewing angles (Supplementary Movie 1).

The material properties of the TiAlN-TiN coating were investigated via x-ray diffraction (XRD). As shown in Fig. 2f, TiN and TiAlN exhibit predominant peaks at $2\theta=36.5°$ and 37.5°, respectively. Both of them have a face centered cubic NaCl-type phase, associated with high hardness, superior mechanical, tribological and anti-oxidation properties [42]. As listed in Table 1, the intrinsic Mohs hardness of TiN and TiAlN reaches 9, much higher than that of common metals and semiconductors. Pencil hardness tests were carried out to identify the hardness of the thin film materials according to international standard ISO15184 (see Methods) [46]. In general, the Mohs hardness of a pencil falls

Fig. 2 a Photograph of 50 nm TiN coating with various thickness of TiAlN films. The surface coloring is insensitive to the substrate materials. Experimentally measured (**b**) and numerically simulated (**c**) reflectance spectra at normal incidence. **d** Chromaticity of experimentally measured (black dots) and numerically simulated spectra (red dots) on the CIE 1931 color space. In simulation, the thickness of TiAlN increases from 0 to 40 nm with a step of 2 nm. **e** Experimentally measured reflectance spectra with oblique incidence. The sample is 20-nm-TiAlN on a 50-nm-TiN film. The dashed line indicates the absorption dips at various incidence angles. **f** X-ray diffraction spectrum of a 20-nm-thick TiAlN on a 50-nm-thick TiN deposited on a sapphire substrate

between 1.5 (10B) and 3 (10H). Therefore, the hardness of the ultrathin coatings (<100 nm) is obviously lower than the intrinsic values of their bulky materials (see Table 1). This is the result of adhesive failure at the coating-substrate interface. For instance, Au, Al have comparable intrinsic Mohs hardness, but Au thin coating has much lower hardness than Al with the same thickness. TiN has a strong adhesion to dielectric substrate [47]. Meanwhile, TiAlN exhibits a strong adhesion to metals through a strong molecular bond [48]. Therefore, compared to the common metallic and semiconductor films, TiN, TiAlN, and TiAlN-on-TiN films cannot be damaged by the hardest pencil (10H). As an alternative, we test them by using sharp corners of various materials, including glass (Mohs hardness 5.5), c-Si (Mohs hardness 6.5), quartz (Mohs hardness 7), sapphire (Mohs hardness 9), and
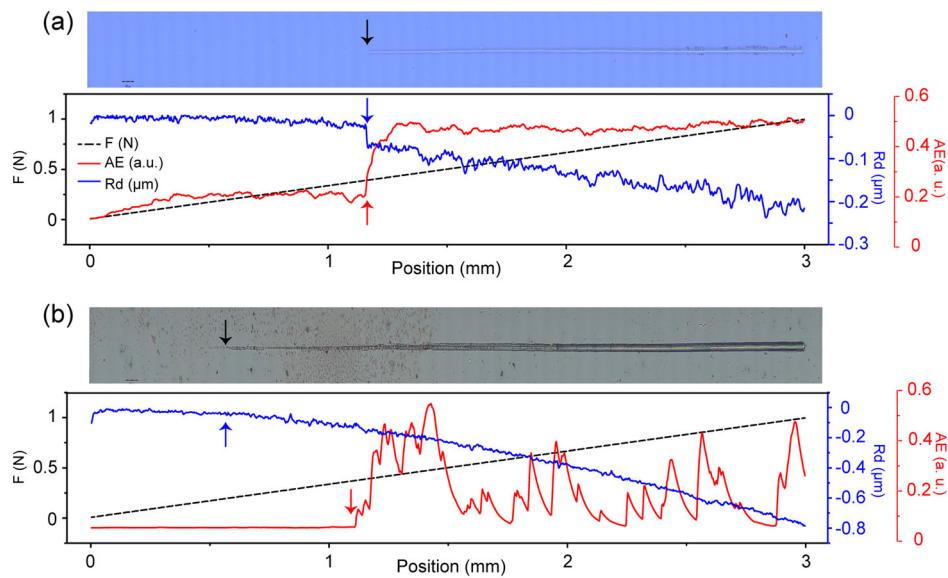
Table 1 Hardness of the common materials versus TiN, AlN and TiAlN for surface coloring. The Bragg coating is a commercially available mirror (EKSMA Optics, 042-5135)

Materials	Hardness [49]	Evaluated thin-film Mohs hardness by scratch tests.
Metallic coatings	angle-independent	Yes
Au	2.5-3	<1.5 (30-nm-thick on c-Si, <10B pencil)
Al	2.5-3	<3 (30-nm-thick on c-Si, 5H pencil)
Cu	3	<3 (30-nm-thick on c-Si, 4H pencil)
Pt	3.5	∼3 (30-nm-thick on c-Si, 10 H pencil)
TiN	9	7-9 (50-nm-thick on sapphire, >quartz; <sapphire)
Semiconductor coatings	angle-independent	Yes
Ge	6	<3 (30-nm-thick on sapphire, 8H pencil)
Si	6-7	<3 (30-nm-thick on sapphire, 8H pencil)
TiAlN	9	7-9 (50-nm-thick on sapphire,>quartz; <sapphire)
Dielectric coatings	angle-independent	No
AlN	9	7-9 (100-nm-thick on glass, >quartz; <sapphire)
Bragg coatings	angle-independent	No
Multilayer dielectrics	∼	5.5-6.3 (6.5μm on glass, <stainless steel)
SM-type coating	angle-independent	Yes
Si(50nm)-Au(50nm)	∼	<2 (substrate: Si wafer, 6B pencil)
Ge(50nm)-Au(50nm)	∼	<2 (substrate: Si wafer, 6B pencil)
Si(50nm)-Cu(50nm)	∼	<2.5 (substrate: Si wafer, 3H pencil)
Si(50nm)-Al(50nm)	∼	<2.5 (substrate: Si wafer, 4H pencil)
Si(50nm)-Ag(50nm)	∼	<2.5 (substrate: Si wafer, 4H pencil)
Si(50nm)-Pt(50nm)	∼	<3 (substrate: Si wafer, 8H pencil)
Si(30nm)-TiN(50nm)	∼	<3 (substrate: Si wafer, 9H pencil)
TiAlN(30nm)-TiN(50nm)	∼	7-9 (substrate: Si wafer, >quartz; <sapphire)
FROC-type coating	angle-independent	Yes
TiAlN-TiN-AlN-TiN	∼	5.5-6.5 (130-nm-thick on sapphire, >glass; <c-Si)

SiC (Mohs hardness 9.5). Test results suggest that TiAlN(20nm)-TiN(50nm) on various substrates is harder than quartz while softer than sapphire (Table 1).

We further quantitatively investigate the wear resistance of the TiAlN-TiN coating using a diamond indenter. To delicately locate the maximum shear stresses at the coating-substrate interface, low loads are applied in this test. The diamond indenter used for scratching the coating exhibits a spheroconical shape with a radius of 20 μm. Figure 3a summarizes the results of the scratch test synchronized with a Panorama image. The coating consists of a 30-nm-TiAlN and a 50-nm-TiN layer on a sapphire substrate. The applied loads increase linearly from 10 mN to 1 N (black curve in Fig. 3a). From the optical microscope image in Fig. 3a, we find that the critical load is ∼400 mN. This is further confirmed by the abrupt increase of acoustic emission (AE, red arrow) and sudden decrease of the residual depth (Rd, blue arrow), which originates from the inelastic deformation of the substrate.
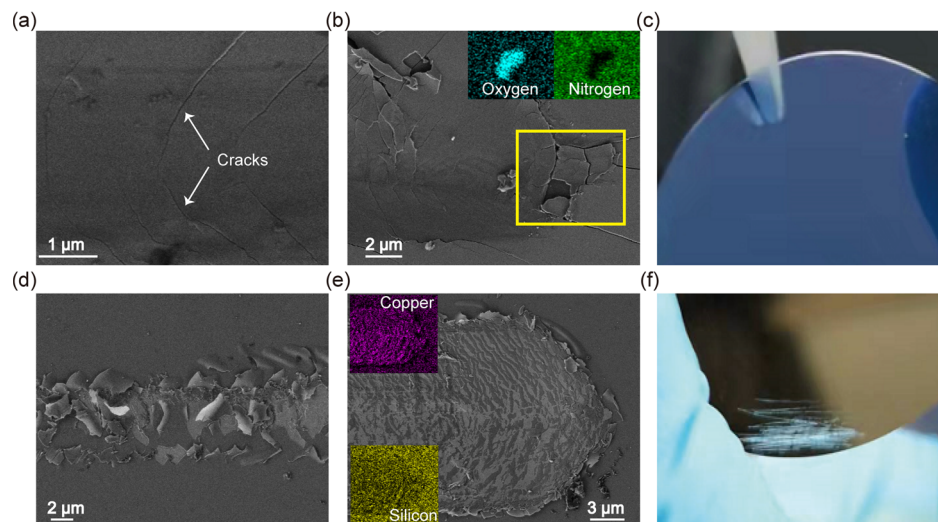
As a comparison, scratch tests on Si(50 nm)-Cu(50nm) coating on a sapphire substrate (Fig. 3b) are carried out. The critical load is evaluated to be ∼140 mN, which, indeed, is much lower than the TiAlN-on-TiN coating. We notice that AE dramatically increases as the load approaches ∼370 mN (red arrow in Fig. 3b). This may suggest the removal of Si coating at 370 mN, and thus the AE arises from the metal or the substrate afterwards. We thus infer that the abrupt rise of AE reflects the property of the sapphire substrate rather than the deposited coating. Moreover, we find that its final Rd is obviously deeper,

Fig. 3 Scratch tests of **a** TiAlN(30nm)-TiN(50nm) coating on a sapphire substrate, and **b** Si(50nm)-Cu(50nm) coating on a sapphire substrate. F: load in the form of mechanical force on the coating; AE: acoustic emission; Rd: residual depth of the sample after the scratch tests. The black arrows indicate the optical microscopy observation of the starting point of damage (critical loads) on the coatings, which is confirmed by the simultaneous measurement of Rd (blue arrows). The Rd rapidly decreases after the critical loads is reached. The red arrows mark the critical loads for the dramatic increase of AE

and the width of the scratch is wider compared to that on the TiAlN-TiN coating. This confirms that the wear resistance of the TiAlN-TiN coating is much better than its Si-Cu counterpart.
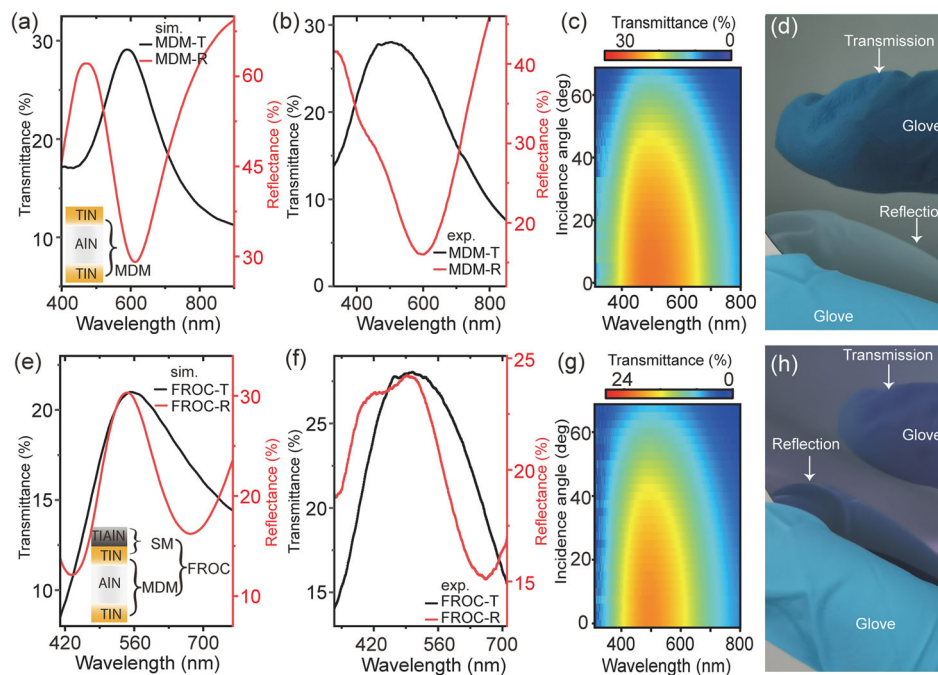
To obtain a deeper insight, the scratches are imaged with scanning electron microscope (SEM). As shown in Fig. 4a, at the critical load, only a few cracks can be observed on the TiAlN-TiN coating. At the end of the scratch (Fig. 4b), the TiAlN coating still exists, accompanied by a handful of tilted cracks, as confirmed by the EDX map of nitrogen (Fig. 4b). Note that the orientation of the cracks is opposite to the drawing direction, which reflects the hardness of the coating, as they originate from the release of tensile

Fig. 4 Scanning electron images and energy dispersive x-ray maps (Insets) of the scratched areas on TiAlN(30nm)-TiN(50nm) coating (**a**,**b**), and on Si(50nm)-Cu(50nm) coating (**d**,**e**). The scratch tests were performed by a diamond indenter. Scratch tests on TiAlN-TiN coating (**c**) and Si-Cu coating (**f**) by a stainless-steel tweezers

stress during the drawing process. In contrast, when drawing on Si-Cu film, it already forms numerous flakes at the critical load (Fig. 4d). At the end of the scratch (Fig. 4e), Si coating has been obviously removed and as a result, the underlying Cu becomes visible from the EDX maps. Therefore, we conclude that for Si coating on metals, its scratch damage mainly attributes to adhesive failure at the Si-metals interface; while the damage of brittle TiAlN originates from cohesive failure. Considering the higher intrinsic hardness of TiAlN than most materials, its wear resistance is self-evident. To illustrate the wear resistance of TiAlN-TiN coating in a more intuitive way, we vigorously scrape the coatings with a tweezers made of stainless steel (hardness 5.5). The conventional coatings consisting of Si on Cu, or on other metals such as Ag, Al and Au are easily damaged (Fig. 4f). With further investigation, we identify that the Si-Cu coating can even be easily removed by fingernails (Mohs hardness 2.5). Conversely, in the case of TiAlN-TiN coating, after application of strong force, still no scratches are visible to the naked eye (Fig. 4c).

Traditionally, the color filters are made of multiple transparent dielectric thin films with quarter-wavelength thickness and different refractive indices, like SiO_2, Al_2O_3 [37, 50]. However, such Fabry-Perot-type Bragg coatings are rather thick, usually with thicknesses up to several micrometers (Table 1). More importantly, they reflect and transmit different colors, and the displayed colors are viewing-angle-dependent (Supplementary Fig. S2-S3). These problems can be solved by FROC, which consists of a SM-type broadband absorber on a MDM-type narrowband absorber. As schematically illustrated in the inset of Fig. 5a, a

Fig. 5 Calculated (**a**) and measured (**b**) reflectance (red curve) as well as transmittance (black curve) spectra of a MDM film stack at normal incidence. Inset: Scheme of MDM film that is made of TiN-AlN-TiN from top to bottom. The thickness of film from the topmost to the bottom layer is TiN = 20 nm, AlN = 70 nm, and TiN = 20 nm, respectively. Calculated (**e**) and measured (**f**) reflectance (red curve) and transmittance (black curve) spectra of a FROC film at normal incidence. Inset: scheme of FROC film consisting of TiAlN-TiN-AlN-TiN. The thickness of each layer from top to bottom is TiAlN = 20 nm, TiN = 20 nm, AlN = 70 nm, and TiN = 20 nm, respectively. Measured transmittance spectra of a MDM film (**c**) and a FROC film (**g**) versus incidence angle. Photographs of a MDM and a FROC coating on glass. The coatings are semi-transparent. The reflection of a glove and transmission of another glove can be observed simultaneously. The MDM reflects and transmits different colors (**d**). The FROC, however, reflects and transmits nearly the same color (**h**)

transparent aluminium nitride (AlN) is employed as the lossless dielectric layer (bandgap ~6.2 eV). Apart from being transparent, it can be conveniently sputtered using the same target materials as TiAlN. Figure 5a and b depicts the complementary behavior of the transmittance and reflectance of the MDM coating, suggesting that it selectively reflects and transmits different colors (Fig. 5d).

By depositing a thin TiAlN layer on the MDM, a FROC coating is obtained, as is shown in the inset of Fig. 5e. It exhibits a modified spectral profile with nearly-identical transmission and reflection (Fig. 5e, f). In consequence, nearly same color of reflection and transmission is observed (Fig. 5h). The structural colors of the FROC are highly sensitive to the dielectric layer. It has been theoretically pointed out that the FROC with high refractive index dielectric layer displays angle-independent colors over a wide angular range, whereas the low-index FROC is highly iridescent [37]. Therefore, another advantage of AlN is that it supports angle-independent structural colors (Fig. 5c, g). Given that more number of layers usually results in a lower hardness, the hardness of the FROC film is slightly lower than the bilayer TiAlN-TiN film (Table 1). Nevertheless, it is still as hard as glass.

Conclusion

In summary, we have demonstrated the use of ceramic materials TiN, AlN and TiAlN to achieve wear-resistant, ultrathin, viewing angle-independent surface colors. Two types of colorful coatings, including SM and FROC, have been illustrated by photographs as well as spectra. Their wear resistance has been experimentally confirmed by scratching tests. Especially, the ultrathin FROC, which transmits and reflects nearly the same viewing angle-independent colors, hold appealing applications in color filters. The combined novel optical property and mechanical robustness depicts a broad application prospect for the proposed coating systems as durable and functional optical devices

Methods

Sample fabrication and characterization

The TiN films were deposited on various substrates by RF magnetron reactive sputtering at 300°C, power of 600 W, and N_2 flow of 14 sccm and Ar of 56 sccm. The TiAlN films were deposited as the same parameters for TiN while the power of Al target is DC 300 W. The AlN films were coated as the same for TiAlN while the Ti target was off. The Au, Cu, Ag, Al films were deposited by the same DC reactive sputter while at room temperature. The amorphous Si was deposited via RF magnetron sputter at room temperature. Coatings on various substrates including single crystalline silicon, sapphire, silica have been tested. The thickness of our films was measured with a profiler (Stylus). According to the measured thickness, the permittivities were retrieved with a variable angle spectroscopic ellipsometer (Woollam). The scanning electron images and energy dispersive x-ray spectroscopy were performed by a field-emission scanning electron microscope (Carl Zeiss, Gemini450). The XRD analysis of the TiAlN-on-TiN coating on sapphire substrate was carried out by Bruker D8 Discover.

Reflectance and transmittance spectra

The reflectance spectra at near-normal incidence were recorded using a Shimadzu UV-VIS-IR spectrophotometer (UV3600Plus+UV2700). The angle-dependent reflectance

and transmittance spectra were taken by an Agilent Cary spectrophotometer (Cary 6000l, UV-Vis-NIR System).

Numerical simulation

The numerical computations were performed by using finite-difference-time-domain (FDTD) method (Lumerical FDTD solutions software package). The light source was a depolarized plane wave spanning from 400 nm to 2 μm. The top and bottom boundaries were perfectly matched layers (PML), while periodic boundary conditions were applied in *x-y* plane. One monitor was set 2 μm above the source to acquire the reflection spectra. The other monitor was set inside the substrate to acquire the transmittance spectra. The permittivities of the materials involved were measured with the aforementioned ellipsometer.

Scratch tests

The pencil hardness test of films was carried out by Mitsubishi pencils under ISO:15184 international standard. Mohs hardness tests by glass, quartz, sapphire and SiC plates follow the procedure: 1, Steady the sample on a table; 2, Hold a plate in one hand to expose a sharp corner; 3, Press the sharp corner onto the sample with some force; 4, Drag the corner across the sample a short distance, without sawing the sample back-and-forth like cutting a piece of wood; 5, Examine the sample surface for evidence of an indentation. The quantitative wear resistance test of the thin films were performed by a scratching tester (Anton Paar Step 100 MCT[3] Micro Combi Tester). The testing method is drawing a diamond indenter with gradual increasing normal load onto the surface. The diamond indenter used for scratching the coatings exhibits a spheroconical shape with a radius of 20 μm. In order to avoid damage of the substrate due to large deformation, a small load ranging from 10 mN to 1 N was applied. After the drawing, a small load of 10 mN was applied to post-scan the scratch and measure the residual depth.

Abbreviations

TiN	titanium nitride
AlN	aluminium nitride(AlN)
TiAlN	titanium aluminium nitride
a-Si	amorphous Silicon
FROC	Fano-resonant optical coating
SM	semiconductor-metal coating
MDM	metal–dielectric–metal
XRD	x-ray diffraction
AE	acoustic emission
SEM	scanning electron microscope
EDX	energy dispersive x-ray spectroscopy
PML	perfectly matched layer

Supplementary Information

The online version contains supplementary material available at https://doi.org/10.1186/s43074-022-00061-5.

Additional file 1. Figure S1. Reflectance spectra of 20 nm TiAlN film coating on 50 nm TiN at various incidence angles. Figure S2. Photographs of a Bragg mirror, also known as multilayer dielectric mirror, viewing at different angles. Figure S3. Photographs of reflection (a) and transmission (b) of a Bragg mirror.

Additional file 2. Video of a Bragg mirror viewing at different angles.

Authors' contributions
M.Q. supervised the whole project. L.-P.S. conceived the experiments. J.G. and J.-H.N. coated the films. J.G. performed the spectral measurement. J.G., W. Y., Q.-N. J. and L.-P.S. wrote the manuscript. All authors participated in the analysis of data and approved the final manuscript.

Availability of data and materials
The experimental data that support the works of this study are available from the corresponding authors on reasonable request.

Declarations

Ethics approval and consent to participate
There is no ethics issue for this paper.

Consent for publication
All authors agreed to publish this paper.

Competing interests
The authors declare that they have no competing interests.

References
1. Kristensen A, Yang JK, Bozhevolnyi SI, Link S, Nordlander P, Halas NJ, Mortensen NA. Plasmonic colour generation. Nat Rev Mater. 2016;2:1–14.
2. Iwata M, Teshima M, Seki T, Yoshioka S, Takeoka Y. Bio-inspired bright structurally colored colloidal amorphous array enhanced by controlling thickness and black background. Adv Mater. 2017;29:1605050.
3. Kumar K, Duan H, Hegde RS, Koh SC, Wei JN, Yang JK. Printing colour at the optical diffraction limit. Nat Nanotechnol. 2012;7:557–61.
4. Odom TW. Printable stained glass. Nat Nanotechnol. 2012;7:550–1.
5. Dean N. Colouring at the nanoscale. Nat Nanotechnol. 2015;10:15–6.
6. Graydon O. A colourful future? Nat Photon. 2015;9:487–8.
7. Shang L, Zhang W, Xu K, Zhao Y. Bio-inspired intelligent structural color materials. Mater Horiz. 2019;6:945–58.
8. Vukusic P, Sambles JR. Photonic structures in biology. Nature. 2003;424:852–5.
9. Anusuyadevi PR, Shanker R, Cui Y, Riazanova AV, Järn M, Jonsson MP, Svagan AJ. Photoresponsive and polarization-sensitive structural colors from cellulose/liquid crystal nanophotonic structures. Adv Mater. 2021;33: 2101519.
10. Højlund-Nielsen E, Clausen J, Mäkela T, Thamdrup LH, Zalkovskij M, Nielsen T, Li Pira N, Ahopelto J, Mortensen NA, Kristensen A. Plasmonic colors: toward mass production of metasurfaces. Adv Mater Technol. 2016;1:1600054.
11. Neubrech F, Duan X, Liu N. Dynamic plasmonic color generation enabled by functional materials. Sci Adv. 2020;6: 2709.
12. Shao L, Zhuo X, Wang J. Advanced plasmonic materials for dynamic color display. Adv Mater. 2018;30:1704338.
13. Zhu X, Vannahme C, Højlund-Nielsen E, Mortensen NA, Kristensen A. Plasmonic colour laser printing. Nat Nanotechnol. 2016;11:325–9.
14. Goh XM, Zheng Y, Tan SJ, Zhang L, Kumar K, Qiu C-W, Yang JK. Three-dimensional plasmonic stereoscopic prints in full colour. Nat Commun. 2014;5:1–8.
15. Ye M, Sun L, Hu X, Shi B, Zeng B, Wang L, Zhao J, Yang S, Tai R, Fecht H-J, et al. Angle-insensitive plasmonic color filters with randomly distributed silver nanodisks. Opt Lett. 2015;40:4979–82.
16. Tan SJ, Zhang L, Zhu D, Goh XM, Wang YM, Kumar K, Qiu C-W, Yang JK. Plasmonic color palettes for photorealistic printing with aluminum nanostructures. Nano Lett. 2014;14:4023–9.
17. Roberts AS, Pors A, Albrektsen O, Bozhevolnyi SI. Subwavelength plasmonic color printing protected for ambient use. Nano Lett. 2014;14:783–7.
18. Liu C, Hong M, Cheung H, Zhang F, Huang Z, Tan L, Hor T. Bimetallic structure fabricated by laser interference lithography for tuning surface plasmon resonance. Opt Express. 2008;16(14):10701–9.
19. Yang B, Liu W, Li Z, Cheng H, Chen S, Tian J. Polarization-sensitive structural colors with hue-and-saturation tuning based on all-dielectric nanopixels. Adv Opt Mater. 2018;6:1701009.
20. Wu Y, Chen Y, Song Q, Xiao S. Dynamic structural colors based on all-dielectric mie resonators. Adv Opt Mater. 2021;9:2002126.
21. Yang W, Xiao S, Song Q, Liu Y, Wu Y, Wang S, Yu J, Han J, Tsai D-P. All-dielectric metasurface for high-performance structural color. Nat Commun. 2020;11:1–8.
22. Liu X, Huang Z, Zang J. All-dielectric silicon nanoring metasurface for full-color printing. Nano Lett. 2020;20:8739–44.

23. Sun S, Zhou Z, Zhang C, Gao Y, Duan Z, Xiao S, Song Q. All-dielectric full-color printing with tio2 metasurfaces. ACS Nano. 2017;11:4445–52.
24. Nagasaki Y, Suzuki M, Hotta I, Takahara J. Control of si-based all-dielectric printing color through oxidation. ACS Photon. 2018;5:1460–6.
25. Vorobyev A, Guo C. Spectral and polarization responses of femtosecond laser-induced periodic surface structures on metals. J Appl Phys. 2008;103:043513.
26. Lütolf F, Stalder M, Martin OJ. Metallized gratings enable color effects and floating screen films by first-order diffraction. Adv Opt Mater. 2015;3:1793–9.
27. Xie T, Xiao X, Li J, Wang R. Encoding localized strain history through wrinkle based structural colors. Adv Mater. 2010;22:4390–4.
28. Geng J, Fang X, Zhang L, Yao G, Xu L, Liu F, Tang W, Shi L, Qiu M. Controllable generation of large-scale highly regular gratings on si films. Light Adv Manuf. 2021;2(3):273–81.
29. Li Z, Butun S, Aydin K. Large-area, lithography-free super absorbers and color filters at visible frequencies using ultrathin metallic films. ACS Photon. 2015;2:183–8.
30. ElKabbash M, Ilker E, Letsou T, Hoffman N, Yaney A, Hinczewski M, Strangi G. Iridescence-free and narrowband perfect light absorption in critically coupled metal high-index dielectric cavities. Opt Lett. 2017;42:3598–601.
31. Mirshafieyan SS, Guo J. Silicon colors: spectral selective perfect light absorption in single layer silicon films on aluminum surface and its thermal tunability. Opt Express. 2014;22:31545–54.
32. Mader S, Martin OJ. Engineering multi-state transparency on demand. Light Adv Manuf. 2021;2(4):1–10.
33. Liu H, Lin W, Hong M. Surface coloring by laser irradiation of solid substrates. APL Photon. 2019;4:051101.
34. Livakas N, Skoulas E, Stratakis E. Omnidirectional iridescence via cylindrically-polarized femtosecond laser processing. Opto-Electron Adv. 2020;3(5):190035–1.
35. Kats MA, Blanchard R, Genevet P, Capasso F. Nanometre optical coatings based on strong interference effects in highly absorbing media. Nat Mater. 2013;12:20–4.
36. Chen S, Rossi S, Shanker R, Cincotti G, Gamage S, Kühne P, Stanishev V, Engquist I, Berggren M, Edberg J, et al. Tunable structural color images by uv-patterned conducting polymer nanofilms on metal surfaces. Adv Mater. 2021;33:2102451.
37. ElKabbash M, Letsou T, Jalil SA, Hoffman N, Zhang J, Rutledge J, Lininger AR, Fann C-H, Hinczewski M, Strangi G, et al. Fano-resonant ultrathin film optical coatings. Nat Nanotechnol. 2021;16:440–6.
38. Limonov MF, Rybin MV, Poddubny AN, Kivshar YS. Fano resonances in photonics. Nat Photon. 2017;11:543–54.
39. Samsonov GV. Mechanical properties of the elements. In: Handbook of the Physicochemical Properties of the Elements. New York: IFI/Plenum; 1968. p. 387–446.
40. Vandeperre L, Giuliani F, Lloyd S, Clegg W. The hardness of silicon and germanium. Acta Mater. 2007;55:6307–15.
41. Santecchia E, Hamouda A, Musharavati F, Zalnezhad E, Cabibbo M, Spigarelli S. Wear resistance investigation of titanium nitride-based coatings. Ceram Int. 2015;41:10349–79.
42. Martin PM. Handbook of Deposition Technologies for Films and Coatings: Science Applications and Technologies. Oxford: Elsevier; 2005.
43. Guler U, Boltasseva A, Shalaev VM. Refractory plasmonics. Science. 2014;344:263–4.
44. Li W, Guler U, Kinsey N, Naik GV, Boltasseva A, Guan J, Shalaev VM, Kildishev AV. Refractory plasmonics with titanium nitride: broadband metamaterial absorber. Adv Mater. 2014;26:7959–65.
45. Panjan M, Gunde MK, Panjan P, Čekada M. Designing the color of altin hard coating through interference effect. Surf Coat Technol. 2014;254:65–72.
46. ISO 15184, Paints and Varnishes: Determination of Film Hardness by Pencil Test. International Organization for Standardization; 1998.
47. Kim W, Kim S, Lee K-S, Lee T, Kim I. Titanium nitride thin film as an adhesion layer for surface plasmon resonance sensor chips. Appl Surf Sci. 2012;261:749–52.
48. Harris S, Doyle E, Vlasveld A, Dolder P. Dry cutting performance of partially filtered arc deposited titanium aluminium nitride coatings with various metal nitride base coatings. Surf Coat Technol. 2001;146:305–11.
49. Pugh S. Mechanical properties of the elements. In: Samsonov GV, editor. Handbook of the Physicochemical Properties of the Elements. New York: IFI Plenum; 1968.
50. Raut HK, Ganesh VA, Nair AS, Ramakrishna S. Anti-reflective coatings: A critical, in-depth review. Energy Environ Sci. 2011;4:3779–804.

Publisher's Note

Springer Nature remains neutral with regard to jurisdictional claims in published maps and institutional affiliations.